

# Ice-sheet contributions to future sea-level change

BY J. M. GREGORY<sup>1,2</sup> AND P. HUYBRECHTS<sup>3,4,\*</sup>

<sup>1</sup>*Department of Meteorology, Centre for Global Atmospheric Modelling, University of Reading, PO Box 243, Reading RG6 6BB, UK*

<sup>2</sup>*Met Office Hadley Centre, FitzRoy Road, Exeter EX1 3PB, UK*

<sup>3</sup>*Departement Geografie, Vrije Universiteit Brussel, Pleinlaan 2, 1050 Brussel, Belgium*

<sup>4</sup>*Alfred-Wegener-Institut für Polar- und Meeresforschung, Postfach 120161, 27515 Bremerhaven, Germany*

Accurate simulation of ice-sheet surface mass balance requires higher spatial resolution than is afforded by typical atmosphere–ocean general circulation models (AOGCMs), owing, in particular, to the need to resolve the narrow and steep margins where the majority of precipitation and ablation occurs. We have developed a method for calculating mass-balance changes by combining ice-sheet average time-series from AOGCM projections for future centuries, both with information from high-resolution climate models run for short periods and with a 20 km ice-sheet mass-balance model. Antarctica contributes negatively to sea level on account of increased accumulation, while Greenland contributes positively because ablation increases more rapidly. The uncertainty in the results is about 20% for Antarctica and 35% for Greenland. Changes in ice-sheet topography and dynamics are not included, but we discuss their possible effects. For an annual- and area-average warming exceeding  $4.5 \pm 0.9$  K in Greenland and  $3.1 \pm 0.8$  K in the global average, the net surface mass balance of the Greenland ice sheet becomes negative, in which case it is likely that the ice sheet would eventually be eliminated, raising global-average sea level by 7 m.

**Keywords:** sea level; ice sheet; Greenland; Antarctica; climate change

## 1. Introduction

During the twentieth century, the rate of global-average sea-level rise was in the range 1.0–2.0 mm yr<sup>−1</sup> (Church *et al.* 2001), with recent analyses for the last 50 years giving values in the upper part of this range (Holgate & Woodworth 2004; Church & White 2006). The ice sheets of Antarctica and Greenland made a relatively small contribution of a few 0.1 mm yr<sup>−1</sup> at most (Church *et al.* 2001; Rignot & Thomas 2002).

In the near-term future, as anthropogenic climate change becomes more pronounced (Cubasch *et al.* 2001), the contribution to sea level from glaciers and

\* Author for correspondence (phuybrec@vub.ac.be).

One contribution of 14 to a Discussion Meeting Issue ‘Evolution of the Antarctic Ice Sheet: new understanding and challenges’.

ice caps will probably be of greater magnitude than that from the ice sheets (Church *et al.* 2001), despite their smaller area. This is because the smaller ice masses generally lie in warmer and wetter climates, giving them a greater sensitivity of ablation to temperature change (Oerlemans & Fortuin 1992). However, the area covered by glaciers and ice caps will rapidly contract as their volume is wasted, and it will preferentially be the ablation area which is lost. Hence, the contribution to sea level from glaciers and ice caps will diminish, while that from surface mass balance of the ice sheets will persist because of their much greater volume and longer time-scales for dynamic adjustment of topography.

Using a three-dimensional thermomechanical ice-sheet model, Huybrechts & De Wolde (1999) found the ice-dynamic and topographic response to contemporary mass-balance perturbations to be negligible for Antarctica and small for Greenland for the twentieth and twenty-first centuries. If so, the main sea-level contribution from the ice sheets due to climate change in these centuries will be given by surface mass-balance perturbation alone, i.e. the change in rates of accumulation by snowfall and ablation (loss of mass) by melting and sublimation. Hence, our principal aim in this paper is to describe a method for calculating the mass-balance perturbation. However, dynamical and topographic adjustment should not be neglected, especially beyond the twenty-first century, and we make an estimate of their effects.

In presently available continental ice-sheet models, the dynamical response has a time-scale of centuries (Huybrechts & De Wolde 1999; Ridley *et al.* 2005). Recent observations (summarized by Alley *et al.* (2005); see references therein) of acceleration of glaciers behind the collapsed Larsen B ice shelf, of ice streams in the Amunden Sea sector of West Antarctica, and of many Greenland outlet glaciers suggest that the time-scales for ice-dynamical changes may be much shorter. Such accelerated flow leads to increased ice discharge into the ocean, but the relevant dynamical processes are not properly understood nor included in continental ice-sheet models, the main difficulty being the treatment of grounding-line migration in response to increased melting of ice by the ocean. This therefore represents an important uncertainty for predictions of sea level, but one which is beyond the scope of this paper to address.

## 2. Scaling method for patterns of climate change

Accurate simulation of ice-sheet surface mass balance requires the use of higher spatial resolution and more detailed representation of processes than is currently possible in climate models, owing principally to computational expense. In particular, AOGCMs used for climate projection on century time-scales do not sufficiently resolve the narrow and steep margins of the ice-sheets (Gregory & Lowe 2000; Huybrechts *et al.* 2004). Orographic uplift is an important influence on the precipitation, and the smooth topography of AOGCMs does not present a sufficient barrier to inland penetration (Ohmura *et al.* 1996; Glover 1999; Murphy *et al.* 2002), giving a weaker precipitation gradient than in reality. Ablation also tends to be overestimated because coarse resolution means that around the margins the area of the ice sheet at low altitude, where melting

preferentially occurs, is exaggerated (Glover 1999; Wild *et al.* 2003). (On Antarctica there is very little ablation, the present climate being too cold.)

Huybrechts *et al.* (2004) developed a two-step downscaling technique for deriving climate-change projections at the spatial resolution needed for ice-sheet mass balance. The technique was employed by Church *et al.* (2001) to make projections for ice sheets based on a range of AOGCMs. The first step produces high-resolution time-dependent climate change data by combining geographical patterns of climate change from high-resolution climate models, generally run for short periods of simulated time, with the time development of change from lower-resolution models, such as HadCM3, which can be run for longer periods. The second step uses the results of the first to perturb an observational climatology, which is used instead of simulations of the present-day climate because even the highest model resolution is insufficient and the results not entirely realistic. Model results are therefore used only for *change* in climate, following the usual assumption that this partly eliminates model systematic errors, which will tend to be common to all climates simulated by the model.

The first step scales the high-resolution simulated climate change according to the ice-sheet area-average change from a time-dependent AOGCM climate integration following the future scenario of interest. The basis for this is the common observation from climate models that the climatological, geographical and seasonal patterns of climate change (with respect to some arbitrary reference climate) tend to stay roughly constant while their amplitudes evolve in time (e.g. Huntingford & Cox 2000), i.e. the climate change at geographical location  $\mathbf{x}$ , month  $m$  and year  $y$  is  $Q(\mathbf{x}, m, y) = F(y)X(\mathbf{x}, m)$ . Thus,  $Q$  is decomposed into  $X$ , which is independent of climate change on multiannual time-scales (but includes the effect of climate change on the seasonal cycle), and  $F(y)$ , which is the time-dependent scaling factor. The scaling technique ignores the presence of internally generated interannual variability, which adds an extra ‘noise’ term to  $Q$ , but provided the variability is small compared with the signal of forced climate change, it can be neglected for practical purposes.

Suppose  $Q_{\text{hi}}(\mathbf{x}, m)$  is the change in the climatological temperature or precipitation simulated by the high-resolution model for some future period with respect to present day. ( $Q_{\text{hi}}$  might be either an absolute or a fractional change—we clarify this below.) The scaling technique estimates that

$$Q(\mathbf{x}, m, y) = FQ_{\text{hi}}(\mathbf{x}, m), \quad F(y) \equiv \frac{\overline{Q_s}(y)}{\overline{Q_d}}, \quad (2.1)$$

where the overline indicates the annual- and area-average change over the ice sheet, which is used as a measure of the magnitude of climate change,  $\overline{Q_s}(y)$  comes from the AOGCM climate scenario integration (‘s’ for ‘scenario’) and  $\overline{Q_d}$  is the area-average climate change for the period simulated by the high-resolution model. If the high-resolution model is an AOGCM, we define  $\overline{Q_d} \equiv \overline{Q_{\text{hi}}}$ . To reduce computational expense, the high-resolution model might instead be an atmosphere-only GCM, driven by boundary conditions (sea-surface temperature and sea ice) from an AOGCM (denoted ‘d’ for ‘driving’). In that case, we calculate  $\overline{Q_d}$  from the driving AOGCM, and, in general,  $\overline{Q_d} \neq \overline{Q_{\text{hi}}}$ ; the high-resolution atmosphere general circulation model (AGCM) is not constrained to simulate the same area-average climate change over the ice-sheet as its driving lower-resolution AOGCM.

The second step generates the perturbed climatology (subscript ‘p’ in equation (2.2)) by applying the local climate change  $Q(\mathbf{x}, m, y)$  estimated from the models to the observed climatology (subscript ‘o’, as in Huybrechts *et al.* (2004) with minor updates). The difference between the two high-resolution climates (future–present, denoted by  $\Delta$ ) is applied using different methods for temperature  $T$  and precipitation  $P$ :

$$\left. \begin{aligned}
 \Delta T_{\text{hi}}(\mathbf{x}, m) \quad Q &\equiv \Delta T, \\
 T_{\text{p}}(\mathbf{x}, m, y) &= T_{\text{o}}(\mathbf{x}, m) + F(y)\Delta T_{\text{hi}}(\mathbf{x}, m), \\
 \Delta P_{\text{hi}}(\mathbf{x}, m) > 0 \quad Q &\equiv \Delta P/P, \\
 P_{\text{p}}(\mathbf{x}, m, y) &= P_{\text{o}}(\mathbf{x}, m) + F(y)\frac{\Delta P_{\text{hi}}(\mathbf{x}, m)}{P_{\text{hi}}(\mathbf{x}, m)}P_{\text{o}}(\mathbf{x}, m), \\
 \Delta P_{\text{hi}}(\mathbf{x}, m) < 0 \quad Q &\equiv \Delta P/(P + \Delta P) \Rightarrow \Delta P/P = Q/(1 - Q) = (1/Q - 1)^{-1}, \\
 P_{\text{p}}(\mathbf{x}, m, y) &= P_{\text{o}}(\mathbf{x}, m) + \left( \frac{P_{\text{hi}}(\mathbf{x}, m) + \Delta P_{\text{hi}}(\mathbf{x}, m)}{F(y)\Delta P_{\text{hi}}(\mathbf{x}, m)} - 1 \right)^{-1} P_{\text{o}}(\mathbf{x}, m),
 \end{aligned} \right\} \quad (2.2)$$

where  $T_{\text{hi}}$  and  $P_{\text{hi}}$  are the high-resolution simulations of the present-day climate and  $F(y)$  is as in equation (2.1). To apply the formulae,  $Q_{\text{hi}}$  must first be interpolated to the higher resolution of the observational climatology.

If the high-resolution model were perfect at its own scale, we would have  $P_{\text{hi}}(\mathbf{x}, m) = P_{\text{o}}(\mathbf{x}, m)$  and  $T_{\text{hi}}(\mathbf{x}, m) = T_{\text{o}}(\mathbf{x}, m)$ . In that case, the perturbed climate for  $F=1$  would be just as simulated by the model, e.g.  $T_{\text{p}}(\mathbf{x}, m) = T_{\text{hi}}(\mathbf{x}, m) + \Delta T_{\text{hi}}(\mathbf{x}, m)$ .

We use ratios for precipitation change because they are likely to be more reliably simulated, given that they tend to have less geographical variation than differences. For instance, the geographical coefficient of variation (area-weighted standard deviation divided by area-weighted average) of annual-average Antarctic precipitation difference  $\Delta P_{\text{hi}}$  simulated by the MIROC3.2 (hires) model is 0.91, while the coefficient of variation of the ratio  $\Delta P_{\text{hi}}/P_{\text{hi}}$  is 0.35. The special treatment for negative local  $\Delta P_{\text{hi}}$  is designed to avoid predicting negative  $P_{\text{p}}$ , which could happen with the  $Q = \Delta P_{\text{hi}}/P_{\text{hi}}$  formulation if  $F$  was large. This situation is actually unlikely to arise, and probably the scaling would not be credible with such large scaling factors. In the limit of small precipitation change  $|F\Delta P_{\text{hi}}/P_{\text{hi}}| \rightarrow 0$ , the two prescriptions for  $P$  give the same result.

### 3. Patterns of precipitation and temperature change

Huybrechts *et al.* (2004) used results of two high-resolution AGCMs (ECHAM4 and HadAM3H in table 1), which had each been integrated for a number of years with surface boundary conditions for each of two periods, one for the present day

Table 1. High-resolution simulations used to obtain temperature and precipitation changes. (The 'WR' column is the ratio of summer warming in Greenland to annual-average warming. The 'yr' column shows the length of each simulation in years.)

model	type	resolution	WR	yr	present	future	references
ECHAM4	AGCM	T106 ( <i>ca</i> 1.125°)	0.71	10	monthly obs. 1971–1980	monthly obs. + change from IS92a simulation of 2041–2050 by ECHAM4/ OPYC3 AOGCM	Wild <i>et al.</i> (2003)
ECHAM5	AGCM	T106	0.90	30	monthly obs. 1961–1990	monthly obs. + change from SRES A2 simulation of 2071–2100 by HadCM3 AOGCM as ECHAM5	Wild <i>et al.</i> (2004)
HadAM3H	AGCM	1.875° × 1.25°	0.86	30	as ECHAM5		Johns <i>et al.</i> (2003)
MIROC3.2 (hires)	AOGCM	T106	0.81	30	pre-industrial simulation	SRES A1B simulation of 2070–2099	Hasumi & Emori (2004)

and one for the future. The boundary conditions for the present day were from observations, and for the future were derived by perturbing an observational climatology using the climate change simulated by time-dependent AOGCM experiments. This is an anomaly technique like the one we employ for the ice sheets, and is done for the same reason, to minimize the effect of model systematic errors in the present-day simulation. Simulations like these are called ‘time slices’, in which a model is integrated for disjointed relatively short periods of simulated time, rather than continuously like an AOGCM.

In this work, we have two more high-resolution simulations available (the details of all four are summarized in [table 1](#)). These are ECHAM5 and MIROC3.2 (hires). The latter is an AOGCM, and therefore does not require driving data for climate change from another model, unlike the other three. The four cases use somewhat different periods for the present-day climate and various scenarios for future climate change. This is unimportant under the assumption that the patterns of climate change are invariant, since the scaling takes these differences into account automatically.

Given four high-resolution models, we are able to make a more thorough assessment of the uncertainty associated with modelling the spatio-temporal patterns of climate change than could be done by [Church \*et al.\* \(2001\)](#), who had only ECHAM4, and [Huybrechts \*et al.\* \(2004\)](#). The common features of annual precipitation increase and summer warming are shown by the ensemble-average pattern, calculated after scaling the four individual patterns to have the same area average over the ice sheet, while the spread of results is measured by the standard deviation ([figure 1](#)).

We show the summer warming (JJA for Greenland, DJF for Antarctica), because it is more relevant than the annual average, since little ablation occurs outside summer. Warming in northern high latitudes is amplified by sea-ice retreat, which has a strong effect in winter, replacing the cold ice surface by open ocean, but less in summer, when melting sea ice will prevent sea surface temperature from rising far above freezing point. Consequently, the summer warming is less than the annual average ([table 1](#)), but since it is an oceanic effect the difference is much less marked for Greenland than for the Arctic in general. The ratio of summer to annual-average warming in these four patterns is  $0.82 \pm 0.08$ , indicating weaker seasonality than the ratios of  $0.74 \pm 0.21$  used by [Gregory \*et al.\* \(2004\)](#), which were derived from AOGCMs.

As noted by [Huybrechts \*et al.\* \(2004\)](#), there are strong similarities among the models. For both ice sheets, the summer warming increases with altitude and is rather small around the coast, probably because the temperature over melting land ice cannot rise above freezing point ([Van de Wal \*et al.\* 2001](#)) and sea-surface warming is also restrained (as above); consistent with this explanation, the effect is weaker for Antarctica, which remains below freezing point over land. The models simulate the near-surface air temperature (usually 2 m height). Changes in this quantity over ice may be quite sensitive to the formulation of the atmosphere boundary-layer scheme. This may represent a substantial but unquantified uncertainty in our calculations.

On Greenland, there are small changes in precipitation on the southeast coast and a large increase in the northeast. On Antarctica, there are smaller increases around the coasts, especially Siple and Adélie, and large increases on the high elevations of East Antarctica. Some similar features occur in the change in

Antarctic precipitation in the simulations of Krinner *et al.* (submitted), with a stretched-grid AGCM having 60 km resolution over Antarctica. Although the patterns agree less strongly among the models than for temperature, the ensemble standard deviation is less than half the ensemble mean, except in the regions of very small increase.

#### 4. Mass-balance perturbation tables

The precipitation and temperature changes are taken as input to the ice-sheet surface mass-balance model of Janssens & Huybrechts (2000). This model uses a degree-day method for ablation, taking into account the retention of meltwater and the phase of precipitation (rain or snow) as a function of temperature. The mass-balance model has a 20 km grid, on which the observational climatology ( $P_o(\mathbf{x}, m)$ ,  $T_o(\mathbf{x}, m)$ ) is constructed, in order to be able to represent the effect of elevation accurately. Since the mass-balance model is purely diagnostic, it can be run independently of the time development from the AOGCM scenario. It is therefore convenient to calculate  $P_p(\mathbf{x}, m)$  for a range of  $\overline{\Delta P_s}$ , using equations (2.1) and (2.2), and  $T_p(\mathbf{x}, m)$  for a range of  $\overline{\Delta T_s}$ , apply these to the mass-balance model, and thus construct a table of mass-balance  $B$  as a function of  $\overline{\Delta P_s}/\overline{P_s}$  and  $\overline{\Delta T_s}$  for each ice sheet. From this we subtract the mass balance computed from the observed climatology. The difference  $\Delta B$  is expressed as a contribution to global-average sea level, i.e.

$$\Delta B(\overline{\Delta P_s}/\overline{P_s}, \overline{\Delta T_s}) = -\frac{1}{A_O \rho_w} \iint (M(P_p, T_p) - M(P_o, T_o)) dm d^2 \mathbf{x}, \quad (4.1)$$

where  $M$  is the surface mass-balance model, the integrals are over the seasonal cycle and the ice-sheet area,  $\rho_w$  is the density of water and  $A_O = 3.62 \times 10^{14} \text{ m}^2$  the area of the ocean. Given  $\overline{\Delta P_s}(y)/\overline{P_s}$  and  $\overline{\Delta T_s}(y)$  from an AOGCM, we can then obtain  $\Delta B(y)$  by looking up the appropriate value in the table, using bilinear interpolation between the discrete set of values of  $(\overline{\Delta P_s}/\overline{P_s}, \overline{\Delta T_s})$  for which the table was computed. A separate table is computed for each high-resolution climate model, reflecting their different  $(P_p, T_p)$  for the same  $(\overline{\Delta P_s}/\overline{P_s}, \overline{\Delta T_s})$ .

In broad terms, the tables for Greenland and Antarctica are of course similar (figure 2 shows the average of the four patterns as a continuous function of  $\overline{\Delta P_s}/\overline{P_s}$  and  $\overline{\Delta T_s}$ ). By construction  $\Delta B = 0$  for zero climate change. Increasing precipitation produces a negative sea-level contribution, as extra mass is accumulated on the ice-sheet. Raising the temperature produces a positive contribution, as extra melting occurs. The colour contours tilt to the right, because the ablation rises nonlinearly with average temperature. The colour contours are vertical in the lower part of the Antarctic table because it is too cold for ablation, so temperature increase has no effect. The uncertainty, shown in line contours, is generally tens of percent, but is easier to appreciate in results presented next.

Considering  $\Delta B(\overline{\Delta P_s}/\overline{P_s})$  with  $\overline{\Delta T_s} = 0$  (a horizontal profile of figure 2 passing through the origin), we see that the negative sea-level contribution increases linearly with precipitation in both Antarctica and Greenland (figure 3*a,c*). The slope for the ensemble of high-resolution models is  $-0.065 \pm 0.012 \text{ mm yr}^{-1} \%^{-1}$

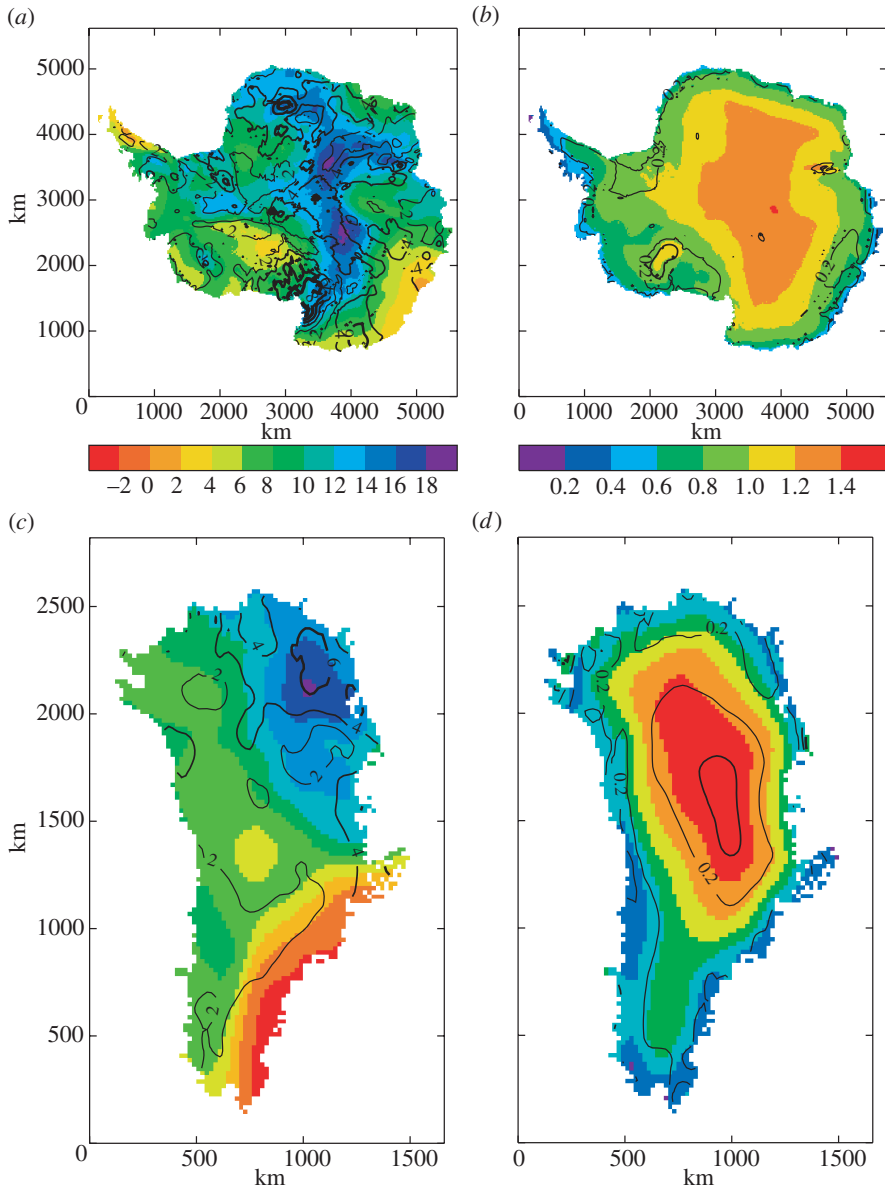
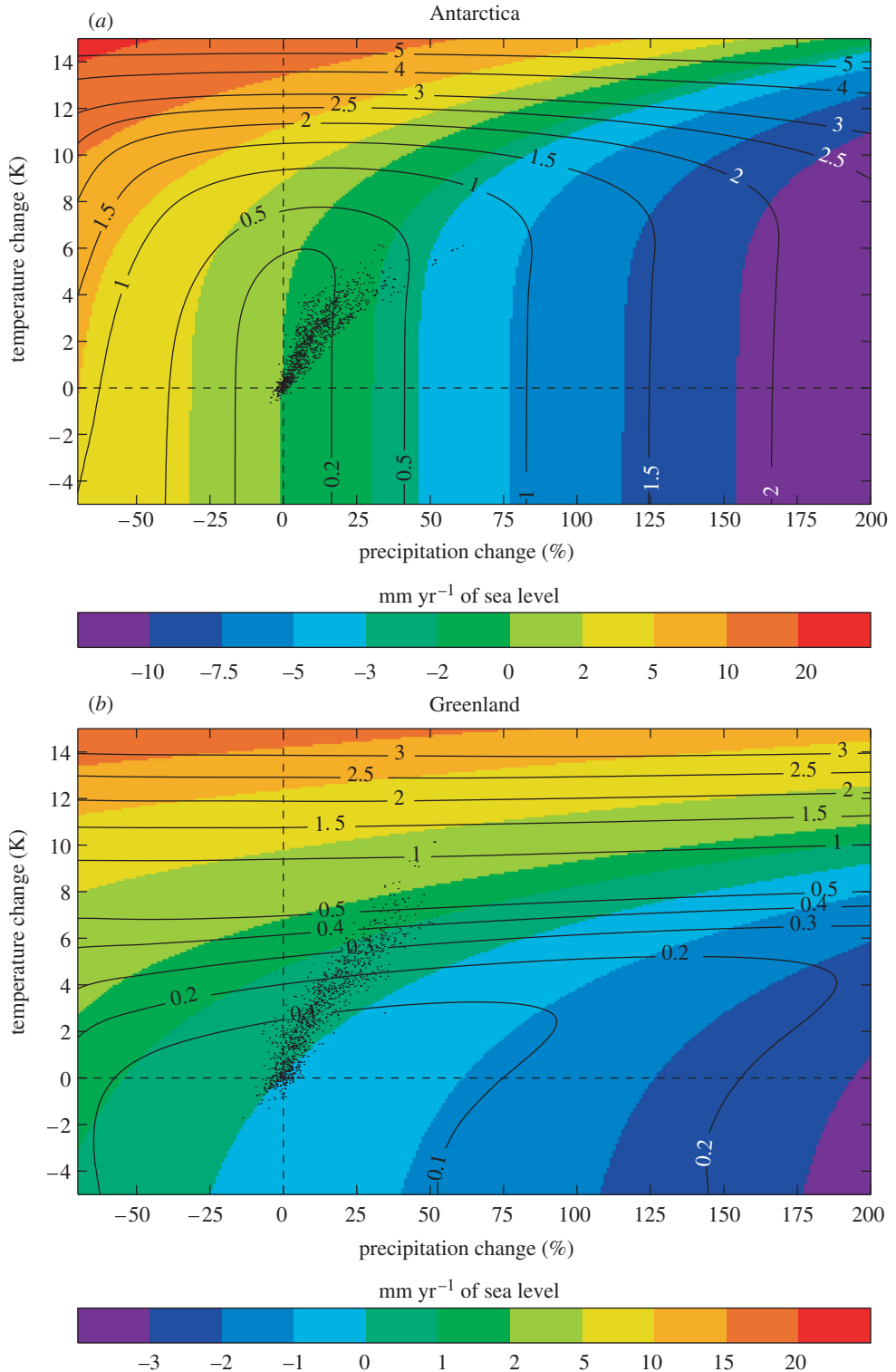


Figure 1. High-resolution patterns of precipitation (%) and temperature (K) change. (a, c) Change in annual-average precipitation in Antarctica and Greenland for  $\overline{\Delta P_{hi}}/P_{hi} = 10\%$ . (b, d) Change in summer-average temperature for  $\overline{\Delta T_{hi}} = 1$  K. In all cases, the colours show the ensemble average and the contour lines the standard deviation within the ensemble. The contour lines are thicker for increasing values and have the same interval as the colours.

Figure 2. (*Opposite.*) Ice-sheet mass-balance perturbation expressed as sea-level equivalent. The perturbation is a function of the annual- and area-average precipitation change  $\overline{\Delta P_s}/P_s$  and temperature change  $\overline{\Delta T_s}$ . The dots indicate the decadal-mean values which occur in the AOGCM scenario experiments considered. The colours show the ensemble average and the contour lines the standard deviation within the ensemble. Note that the two plots do not use the same colour scale.

Figure 2. (*Caption opposite.*)

(average  $\pm$  s.d.) for Antarctica and  $-0.016 \pm 0.001$  mm yr $^{-1}\%$  $^{-1}$  for Greenland. The standard deviations are *ca* 20 and 10% of the averages.

The different patterns have different slopes, because the dependence of  $\Delta B$  is on  $\overline{\Delta P_s/P_s}$ , and the two downscaling steps translate a given value of  $\overline{\Delta P_s/P_s}$  into different absolute values of total precipitation change over the ice sheet. On some grounds, for example the energy balance, one would argue that the absolute precipitation change should be conserved by the downscaling. Unfortunately, it is not possible at the same time to preserve both the area-average absolute and the local fractional changes, unless the model is perfect (giving an exact simulation of the observed  $P_o$ ). If the high-resolution present-day climatology had a uniform precipitation field, any field of percentage change with a given area average would imply the same absolute area-average precipitation change in the model; when applied to the very non-uniform  $P_o(\mathbf{x})$ , however, they give different absolute changes. For comparison, we show (dotted lines in figure 3*a,c*) the accumulation calculated by the mass-balance model for the observed climatology (5.6 mm yr $^{-1}$  of sea-level fall for Antarctica and 1.5 mm yr $^{-1}$  for Greenland) multiplied by the percentages on the horizontal axis. These relationships lie within the ensemble of results from the high-resolution patterns. Given this consistency, we conclude that the conflict between conserving fractional and absolute changes in the downscaling is not too serious for these high-resolution models.

For Greenland, we show the average  $\Delta B(\overline{\Delta P_s/P_s})$  for  $\overline{\Delta T_s} = 1$  K (dashed line in figure 3*c*). The slope is very similar to that for  $\overline{\Delta T_s} = 0$  K, indicating there is little interaction between  $\overline{\Delta P_s/P_s}$  and  $\overline{\Delta T_s}$  changes, but the line is displaced on account of the increased ablation. For Antarctica, the lines are coincident, as ablation remains insignificant (apparent also from figure 2*a*).

Considering  $\Delta B(\overline{\Delta T_s})$  with  $\overline{\Delta P_s/P_s} = 0$  (a vertical profile of figure 2 passing through the origin), we see that the positive sea-level contribution increases more rapidly than linearly with temperature for both Antarctica and Greenland (figure 3*b,d*), due to the behaviour of the ablation scheme, but for Antarctica there is no ablation until  $\overline{\Delta T_s}$  is large. The spread of the high-resolution models is due to their different patterns of  $\Delta T_{hi}(\mathbf{x}, m)$ , and for Greenland it is a larger proportional systematic uncertainty than that associated with the precipitation patterns. For instance, for Greenland, the tangent slopes  $\partial \Delta B / \partial \overline{\Delta T_s} = 0.16 \pm 0.04$  mm yr $^{-1}$  K $^{-1}$  at  $\overline{\Delta T_s} = 1$  K and  $0.54 \pm 0.12$  mm yr $^{-1}$  K $^{-1}$  at  $\overline{\Delta T_s} = 6$  K, representing a 20–25% uncertainty.

We show also the average  $\Delta B(\overline{\Delta T_s})$  with  $\overline{\Delta P_s/P_s} = 20\%$  (dashed lines). For Greenland, this line is quite closely parallel to that for  $\overline{\Delta P_s/P_s} = 0\%$ , confirming the lack of interaction between  $\overline{\Delta P_s/P_s}$  and  $\overline{\Delta T_s}$ , but displaced because of the greater accumulation. For Antarctica, it becomes parallel at large  $\overline{\Delta T_s}$ . The negative sea-level effect of  $\overline{\Delta P_s/P_s}$  is smaller at higher  $\overline{\Delta T_s}$  in general, because more of the extra precipitation falls as rain; the detailed behaviour depends on the distribution of precipitation and temperature with altitude.

## 5. Future changes in ice-sheet mass

Equipped with the mass-balance perturbation tables, we can derive time-series of mass-balance changes for the ice sheets from AOGCM simulations of future climate change. We use decadal averages from a range of AOGCMs (table 2),

Table 2. Results from AOGCMs used for ice-sheet mass projections. (The columns labelled with SRES scenario names give the last year (to the nearest decade) available in the simulation. The columns marked  $r$  are correlation coefficients and those marked  $s$  are slopes, for the temporal variation of decadal averages of  $\overline{\Delta P_s/P_s}$  (fractional change in ice-sheet average precipitation) versus  $\overline{\Delta T_s}$  (ice-sheet average temperature change), labelled ' $\overline{\Delta P_s/P_s}$ ', and  $\overline{\Delta T_s}$  versus  $\Delta T_g$  (global-average temperature change), labelled ' $\overline{\Delta T_s}$ '. The slopes for the former are in  $\% K^{-1}$  and for the latter in  $K K^{-1}$ . The final line shows the mean and standard deviation of slopes. \*Excluding GISS-AOM.)

AOGCM				Antarctica				Greenland			
	A1B	A2	B1	$\overline{\Delta P_s/P_s}$		$\overline{\Delta T_s}$		$\overline{\Delta P_s/P_s}$		$\overline{\Delta T_s}$	
				$r$	$s$	$r$	$s$	$r$	$s$	$r$	$s$
BCCR-BCM2.0	—	2100	2100	0.98	5.8	0.99	1.3	0.85	2.7	0.99	1.4
CGCM3.1 (T47)	2300	2100	2300	0.99	7.8	0.99	1.1	0.95	6.7	0.98	1.5
CNRM-CM3	2250	2100	2250	0.86	2.7	0.97	0.8	0.92	5.0	0.98	1.4
CSIRO-Mk3.0	2200	2100	2250	0.99	7.2	0.99	1.2	0.95	5.6	0.96	1.7
ECHAM5/MPI-OM	2200	2100	2200	0.98	6.2	0.99	1.0	0.96	5.0	0.99	1.4
FGOALS-g1.0	2200	—	2200	0.99	5.8	0.99	1.0	0.99	5.0	0.99	2.3
GFDL-CM2.0	2300	2100	2300	0.98	5.1	0.98	1.0	0.97	6.3	0.98	1.5
GFDL-CM2.1	2300	2100	2300	0.95	4.1	0.96	0.8	0.88	4.3	0.97	1.1
GISS-AOM	2100	—	2100	0.93	2.7	0.99	1.4	-0.45	-1.5	0.92	0.9
GISS-EH	2100	—	—	0.97	3.7	0.97	0.8	0.87	3.8	0.99	1.2
GISS-ER	—	2100	2300	0.98	4.5	0.98	1.0	0.75	3.6	0.98	1.2
INM-CM3.0	2200	2200	2200	0.96	5.2	0.99	1.0	0.95	4.9	0.99	1.2
IPSL-CM4	2180	2100	2180	0.95	3.1	0.98	0.8	0.94	3.9	0.99	1.2
MIROC3.2 (medres)	2300	2100	2300	0.98	5.0	0.99	0.9	0.97	5.2	0.99	1.7
MRI-CGCM2.3.2	2200	2100	2200	0.99	4.5	0.99	1.0	0.94	3.8	0.99	1.6
PCM	2100	2100	2300	0.99	5.4	0.98	1.4	0.97	4.8	0.98	2.3
UKMO-HadCM3	2100	2100	2100	0.96	5.1	0.99	1.2	0.88	4.3	0.98	1.4
UKMO-HadGEM1	2100	2100	—	0.99	7.3	0.99	1.2	0.98	5.7	0.96	1.7
s stats				5.1 ± 1.5		1.1 ± 0.2		*4.7 ± 1.0		1.5 ± 0.4	

whose results have been assembled for analysis as part of the forthcoming Fourth Assessment Report of the Intergovernmental Panel on Climate Change (IPCC). The precise areas defining the ice sheets for evaluating  $\overline{\Delta P_s/P_s}(y)$  and  $\overline{\Delta T_s}(y)$  differ among the various AOGCMs, since each has its own horizontal grid and land–sea mask, and not all distinguish between ice sheet and ice-free land. For simplicity, we used the entire area of Greenland and Antarctica in each model, up to the coast, but found that restricting the mask more exactly to the area of the real ice sheet made practically no difference.

The simulations begin in the late nineteenth or start of the twentieth century and have historical changes in greenhouse-gas and sulphate aerosol concentrations up to the end of the twentieth century (in some cases also including solar variability and volcanic aerosol), then follow Special Report on Emissions Scenarios (SRES) scenarios A1B, B1 and A2 for anthropogenic emissions up to 2100. These three scenarios are among those developed by Nakićenović *et al.* (2000), which were used to make projections in the Third Assessment Report of

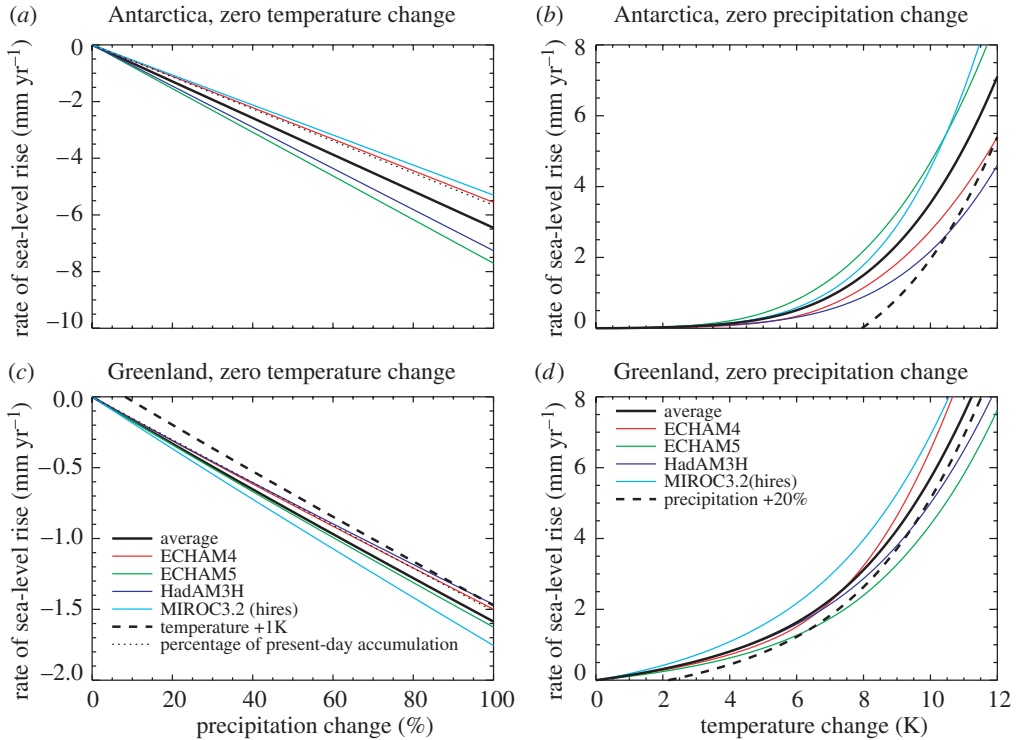


Figure 3. Mass-balance perturbations. (a, c)  $\Delta B$  as a function of precipitation change  $\overline{\Delta P_s}/\overline{P_s}$  for  $\overline{\Delta T_s} = 0$  K. (b, d)  $\Delta B$  as a function of temperature change  $\overline{\Delta T_s}$  for  $\overline{\Delta P_s}/\overline{P_s} = 0$ . The coloured lines show  $\Delta B$  for each of the four high-resolution models, and the solid black line their average. In (a) the magenta and red lines are practically coincident, and in (c) the dark blue and black.

the IPCC. They follow a variety of assumptions for future demographic, economic and technological development. Many of the AOGCM experiments continue from 2100 for up to 200 years with constant atmospheric composition as for 2100, to investigate the effect of ‘stabilization’, although an abrupt transition to fixed composition is of course unrealistic.

In these experiments, the late nineteenth century is assumed to be a steady state. In fact, the climate is never steady owing to natural forcing (solar and volcanic), but these influences are small compared with the anthropogenic forcing even during the twentieth century (e.g. *Stott et al. 2000*), and certainly beyond, so the assumption is reasonable. As is usual, the climate change ( $\overline{\Delta P_s}/\overline{P_s}$ ,  $\overline{\Delta T_s}$ ) is obtained by comparing the scenario experiment of the AOGCM with a control experiment running in parallel with constant initial atmospheric composition; this procedure is followed in order to eliminate any ‘drift’ in the simulated climate. We compute ( $\overline{\Delta P_s}/\overline{P_s}$ ,  $\overline{\Delta T_s}$ ) from decadal averages.

The mass-balance perturbations were calculated for the difference between the present-day and some future climate, but the scenario experiments give us differences between the late nineteenth century and the future. This does not matter so long as  $\Delta B$  depends linearly on  $\overline{\Delta P_s}/\overline{P_s}$  and  $\overline{\Delta T_s}$ . We have seen that this is the case for  $\overline{\Delta P_s}/\overline{P_s}$  but not for  $\overline{\Delta T_s}$ . However, the change in climate

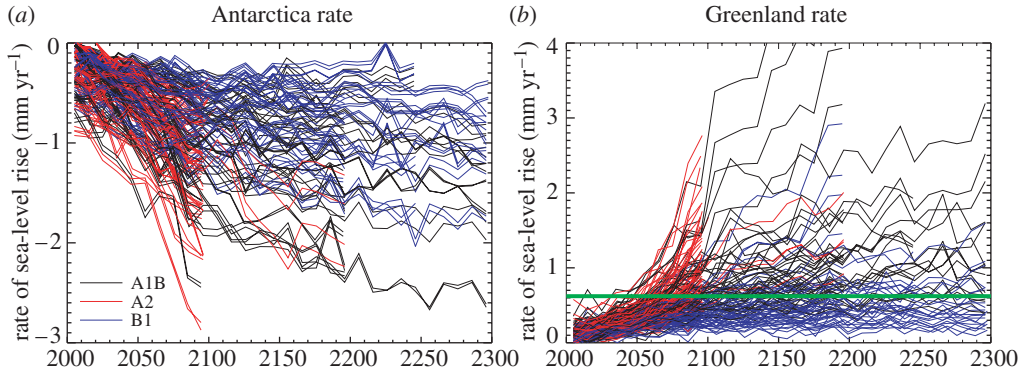


Figure 4. Rates of contribution to sea level ( $\text{mm yr}^{-1}$ ) from ice sheets due to surface mass-balance change. Results are calculated for all available combinations of AOGCM, high-resolution model and emissions scenario (distinguished by line colour), and expressed as sea-level equivalent. The horizontal green line in (b) indicates the magnitude  $|B_0|$  of the present-day surface mass balance of the Greenland ice sheet.

during the twentieth century is much smaller than the future change, so this inconsistency is not serious.

It is a common result of these AOGCMs, as also of those used by Church *et al.* (2001), that precipitation change  $\overline{\Delta P_s}$  rises linearly with temperature change  $\overline{\Delta T_s}$  over each ice sheet. According to the analysis by Van Lipzig *et al.* (2002) using a regional model for Antarctica, greater moisture convergence from lower latitudes in the warmer atmosphere and increased evaporation in the vicinity of the continent owing to higher sea-surface temperatures and to reduced sea-ice extent are all significant factors in the precipitation increase. Reasons for increases in humidity and evaporation in a higher- $\text{CO}_2$  climate are discussed by Allen & Ingram (2002). The linearity of the relationship is an instance of the general scaling of climate change responses noted above (Huntingford & Cox 2000).

Taking the decadal averages from all the scenarios together, the correlation between  $\overline{\Delta P_s}/\overline{P_s}$  and  $\overline{\Delta T_s}$  is at least 0.95 for Antarctica in all the AOGCMs, and at least 0.87 for Greenland in all except GISS-ER and GISS-AOM (table 2). The latter, in particular, is unusual in showing no correlation. The slope is *ca*  $5\% \text{ K}^{-1}$  for both ice sheets; the distributions are  $5.1 \pm 1.5\% \text{ K}^{-1}$  for Antarctica and  $4.7 \pm 1.0\% \text{ K}^{-1}$  for Greenland, excluding GISS-AOM.

Kapsner *et al.* (1995) report that Greenland ice cores indicate no significant relationship between precipitation and temperature within the Holocene. However, Holocene climate variability on centennial time-scales produced by internal variability, and natural forcing may not be a good analogue for future climate change induced by greenhouse gases. Gregory *et al.* (in press) suggest on the evidence of a 500-year integration of HadCM3 that natural forcing may indeed produce a weaker relationship between  $\overline{\Delta P_s}$  and  $\overline{\Delta T_s}$ .

Because  $\overline{\Delta P_s}/\overline{P_s} \propto \overline{\Delta T_s}$ , the locus of points for decadal-average climate change simulated by the AOGCMs slants up and right on the plots of  $\Delta B(\overline{\Delta P_s}/\overline{P_s}, \overline{\Delta T_s})$  (figure 2). This tends to keep the Antarctic contribution to sea level in the negative region of  $\Delta B$  (net positive surface mass-balance change) due to

increased accumulation. Increased ablation in Greenland is mitigated but not overwhelmed by the precipitation increase, so the Greenland contribution to sea level remains in the positive region.

To compute the rates of the contributions to sea level from ice sheets due to surface mass-balance change, we evaluate  $\Delta B(\overline{\Delta P_s}/\overline{P_s}, \overline{\Delta T_s})$  for every AOGCM scenario (18 AOGCMs and three scenarios, though not all models have run all scenarios) using every table (four for each ice sheet, i.e. one from each high-resolution model). The uncertainty associated with the calculation of surface mass-balance change amounts to about 20% for Antarctica and 35% for Greenland, the latter being the combination in quadrature of the pattern uncertainties with a 10% uncertainty on the ablation for the surface mass-balance scheme itself (Church *et al.* 2001). With only one pattern available, Church *et al.* (2001) could not evaluate the associated uncertainty, which they underestimated as 10% for Greenland and nil for Antarctica.

Time-series of the rates of contribution to sea level (figure 4) show the opposite tendencies of the ice sheets. The Antarctic contribution is increasingly negative with time, while the Greenland contribution is increasingly positive. However, they do not balance; their sum is positive in some cases, negative in others.

The three SRES scenarios which have been run by the AOGCMs do not cover the whole range of SRES uncertainty; scenario B1 has among the smallest greenhouse-gas emissions, but there are other scenarios which have larger emissions than A1B or A2—in the projections of Cubasch *et al.* (2001) and Church *et al.* (2001), the greatest climate and sea-level change resulted from scenario A1FI, which has not been covered here. Moreover, we do not have the same length or number of simulations with each of the scenarios; the A2 scenarios are shortest, in general, and the B1 longest (table 2). We have made no attempt to weight the scenarios to remove these biases or assign probabilities to the AOGCMs. Our purpose in this work is only to propose a methodology for making projections.

## 6. Vulnerability of the Greenland ice sheet

The rate of change of mass of the Greenland ice sheet can be written as

$$\frac{dM_G}{dt} = B - D = S - R - D. \quad (6.1)$$

Estimates from multidecadal averages (Church *et al.* 2001) indicate that about half of the accumulation  $S$  (best estimate  $520 \pm 26$  Gt yr<sup>-1</sup>) is balanced by ablation, i.e. runoff  $R$  ( $297 \pm 32$  Gt yr<sup>-1</sup>), the net surface mass-balance  $B = S - R$  ( $225 \pm 41$  Gt yr<sup>-1</sup>, equivalent to 0.62 mm yr<sup>-1</sup> of sea level) being removed by ice discharge  $D$  across the grounding line.

Altimetric observations for recent years show that  $dM_G/dt < 0$ , i.e. the ice sheet is losing mass (predominantly around the margins), at a rate equivalent to 0.13 mm yr<sup>-1</sup> of sea-level rise for the 1990s (Rignot & Thomas 2002) and  $0.22 \pm 0.03$  mm yr<sup>-1</sup> for 1997–2003 (Krabill 2004). The rate of mass change deduced from satellite measurements of the gravity field during 2002–2004 gives  $0.22 \pm 0.06$  mm yr<sup>-1</sup> (Velicogna & Wahr 2005). The imbalance is caused by a combination of changes in all the terms. From previous sections, we would expect twentieth-

century climatic warming to have led to greater  $R$ , exceeding the accompanying increase in  $S$  for the ice sheet as a whole, although in the interior the accumulation increase should produce a thickening, which has been confirmed for 1992–2003 from satellite altimetry (Johannessen *et al.* 2005).

Using climate-change results from the AOGCMs of the IPCC Third Assessment Report, Huybrechts *et al.* (2004) found an average twentieth-century mass loss equivalent to  $0.06 \text{ mm yr}^{-1}$  sea-level rise due to contemporary climate change. Our present ensemble of models gives  $0.04 \pm 0.03 \text{ mm yr}^{-1}$  for the twentieth century and  $0.11 \pm 0.06 \text{ mm yr}^{-1}$  for the 1990s. An increasing imbalance is consistent with greater warming, but since there is probably substantial interannual variability and the AOGCM simulations of the twentieth century will not exactly reproduce historical variations, we cannot expect precise agreement. Results for the surface mass balance obtained from a high-resolution regional climate model indicate roughly compensating trends in  $S$  and  $R$  over 1988–2004 (Box *et al.* in press), while calculations on a 5 km grid using meteorological reanalyses suggest an increasingly negative net surface mass-balance  $B$  over recent decades (Hanna *et al.* 2005). In both cases, the mass loss is smaller than measured by altimetry because of the contribution from accelerated ice discharge  $D$  (see §8).

While the surface mass-balance  $B$  is positive, the Greenland ice sheet will occupy essentially the whole of the island; if there were no discharge with  $B > 0$ , the ice sheet would expand until it reached the sea. Increasing ablation will produce marginal thinning; a consequently reduced  $B$  could be compensated by reduced  $D$  with little contraction of area. However, if  $B$  reaches zero, the ice sheet must retreat from the coast to reduce  $D$  to zero. If  $B$  becomes negative, loss of mass in the peripheral ablation zone will cause the ice sheet to contract in area, while transfer of mass from the central accumulation zone to feed the ablation zone will lower the surface around the margins, causing the ablation area to extend inwards. Eventually, the ice sheet will be eliminated, except those parts grounded at high altitude. Complete removal of the ice sheet would raise global-average sea level by 7.2 m (Church *et al.* 2001).

Although the detailed response of the ice sheet to surface mass balance depends on dynamics (§8), the argument suggests that  $B=0$  is a practical threshold for the viability of the ice sheet. In §5, we calculated the surface mass-balance perturbation  $\Delta B(y)$  using the high-resolution patterns and the AOGCM  $\Delta T_s(y)$  and  $\Delta P_s(y)$  time-series. The threshold  $B=0$  is reached when  $\Delta B = -B_0$ , where  $B_0$  is the surface mass balance in the unperturbed climate. We take  $|B_0| = 0.62 \text{ mm yr}^{-1}$ , the long-term estimate of Church *et al.* (2001). ( $B_0 > 0$  in  $\text{Gt yr}^{-1}$ , but less than zero in sea-level equivalent.)

Using a degree-day model for ablation and assuming that precipitation increases with temperature at  $5.3\% \text{ K}^{-1}$ , Huybrechts *et al.* (1991) found that a seasonally and geographically uniform warming exceeding 2.7 K over the Greenland ice sheet would increase ablation sufficiently to reach the  $\Delta B$  threshold. Greve (2000) simulated the evolution of the ice sheet with a range of seasonally and geographically uniform warmings, and produced a similar result that a warming of between 2 and 3 K is required to bring about a substantial loss of volume within 1000 years (fig. 3 of Greve (2000)).

We saw above (figure 1) that the warming simulated by the high-resolution GCMs in the ablation zone of the ice sheet is less than the average over Greenland.

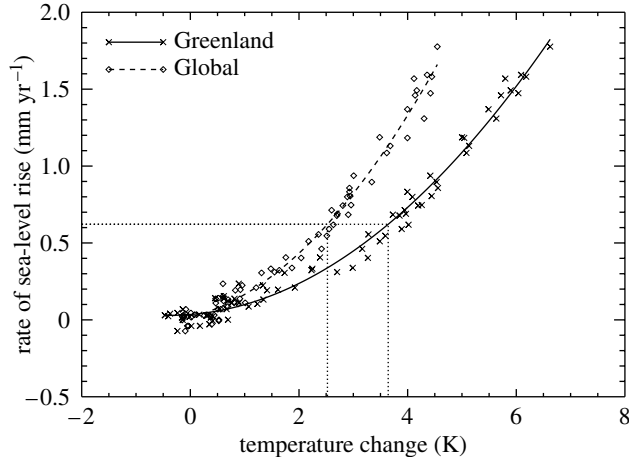


Figure 5. Example of the dependence of Greenland surface mass balance on temperature. The example is for the ECHAM5/MPI-OM AOGCM with climate-change patterns from the MIROC3.2 (hires) model. The symbols show the variation of the surface mass-balance perturbation  $\Delta B$ , expressed as sea-level equivalent, with either the Greenland annual- and area-average temperature change  $\overline{\Delta T_s}$  or the global-average temperature change  $\Delta T_g$ . The solid and dashed lines are quadratic fits. The dotted line intercepts the vertical axis at the magnitude  $|B_0|$  of the present-day surface mass balance of the Greenland ice sheet.

Furthermore, the ablation increase is mostly affected by the summer warming, which is smaller than the annual-average warming (§3). We would therefore expect that reducing the surface mass balance to zero will require a greater area- and annual-average warming  $\overline{\Delta T_s}$  than suggested by these earlier studies, which assumed the warming to be seasonally and geographically uniform. From our results, the warming required for zero surface mass balance must indeed generally be higher than 2.7 K, because  $\overline{\Delta T_s}$  passes this level by the 2090s in 90% of the AOGCM experiments we have considered, and eventually in all of them which continue to 2300, but the  $\Delta B$  threshold is not reached in all cases.

We use the time-series of  $\Delta B(y)$  and  $\overline{\Delta T_s}(y)$  from §5 to examine  $\Delta B(\overline{\Delta T_s})$  for each combination of AOGCM and high-resolution pattern for Greenland. For each case, the dependence can be fitted well by a quadratic function (figure 5 shows an example), from which we can calculate  $\overline{\Delta T_s}$  for  $\Delta B = -B_0$ . In most cases, this amounts to an interpolation within the data available; in 18% of cases it is an extrapolation. In 7% of cases the quadratic fit, when extrapolated, does not reach the threshold, because ablation is not increasing fast enough to outweigh accumulation. The frequency distribution of  $\overline{\Delta T_s}$  over Greenland required to reach the  $\Delta B$  threshold has a 95% confidence interval of 3.2–6.5 K and is somewhat skewed towards lower values, with a mean of 4.5 K and standard deviation of 0.9 K (figure 6). These warmings are with respect to the climate of the late nineteenth century, since that is assumed to be the state of zero perturbation. Although the threshold is derived from AOGCM time-series, the method of calculating the mass-balance perturbation looks only at the dependence of  $\Delta B$  on  $\overline{\Delta T_s}$  and not on its history, so the threshold does not apply to any particular date.

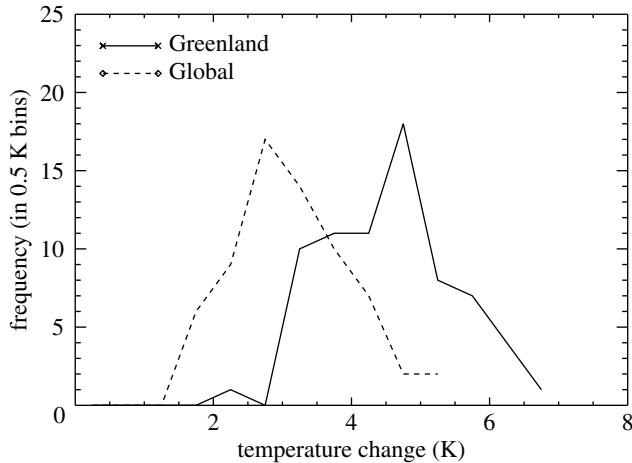


Figure 6. Warming required for a Greenland surface mass balance of zero. Frequency distributions formed by combining every AOGCM with every high-resolution model. The two distributions are of Greenland annual- and area-average temperature change  $\overline{\Delta T_s}$  and the global-average temperature change  $\Delta T_g$ .

Gregory *et al.* (2004) examined projections of Greenland summer temperature change made using methods from the IPCC Third Assessment Report (Cubasch *et al.* 2001) for scenarios which stabilize  $\text{CO}_2$  at concentrations between 450 and 1000 p.p.m. Since the majority (24 out of 35, or 69%) of these projections passed the warming threshold of 2.7 K, they concluded that the Greenland ice sheet is likely to be eliminated. Direct comparison with the present results is unfortunately not possible because the scenarios and AOGCMs are not the same, but we would expect a smaller proportion of cases to pass the mass-balance threshold using the present method. The qualitative conclusion may stand, however, when due consideration is given to the complete range of scenarios.

## 7. Relationship to global climate change

Extension of the results to other scenarios may depend on the use of simple climate models, which project only global-average temperature change  $\Delta T_g$ , as was done by Cubasch *et al.* (2001). Hence, we need to relate  $\Delta B$  for each ice sheet to  $\Delta T_g$ . We find that  $\overline{\Delta T_s} \propto \Delta T_g$ , in line with the scaling behaviour generally found for AOGCM climate-change results. The correlation coefficient  $r \geq 0.96$  in nearly every case (table 2). Quadratics can therefore be fitted satisfactorily to  $\Delta B(\Delta T_g)$ , as for  $\Delta B(\overline{\Delta T_s})$  (an example is shown in figure 5), offering a practical way to estimate mass-balance changes using simple climate models.

The temperature change in Antarctica is not systematically different from the global average; the regression slopes of  $\overline{\Delta T_s}$  versus  $\Delta T_g$  are  $1.1 \pm 0.2 \text{ K K}^{-1}$  (table 2). However, Greenland experiences more warming than the global average, with regression slopes of  $1.5 \pm 0.4 \text{ K K}^{-1}$ , because of the amplification of warming at high northern latitudes due to retreat of seasonal snow and sea ice. The AOGCMs used by Church *et al.* (2001) had an average of 1.8 for the twenty-first century, while Chylek & Lohmann (2005) estimated 2.2 from station data

for the last 30 years. Consequently, the threshold for zero mass balance for Greenland is lower in  $\Delta T_g$  than in Greenland  $\Delta T_s$ . The 95% confidence interval for the  $\Delta T_g$  threshold is 1.9–5.1 K for this set of models, with mean 3.1 K and standard deviation 0.8 K (figure 6).

## 8. Influence of changing ice dynamics and topography

The calculations we have described in this paper are for surface mass-balance change only, i.e. with fixed surface topography or ‘geometry’, and unchanging ice flow. This gives a strictly accurate rate of change of ice mass only for an instantaneous change in climate. A change in surface mass balance implies a rate of change of surface altitude, and this may affect the mass balance. As the topographic change becomes more pronounced, it will alter the gravitational driving stresses, and hence the ice flow.

Huybrechts & De Wolde (1999) carried out experiments in which a thermomechanical ice-sheet model was coupled to a simple climate model, using a similar surface mass-balance scheme to that employed here, but with temperature change that depended only on latitude and precipitation change on temperature change. For three different CO<sub>2</sub> concentrations they simulated the evolution of each ice sheet over 1000 years in three ways: with evolving topography and dynamics (referred to as ‘dynamic’); with evolving topography but unchanging ice flow (‘static’); and with both topography and ice flow constant (‘fixed’). The last considers surface mass balance only, as in the present paper. We can use their results to quantify the effects we are omitting, by examining how much the dynamic calculation of sea-level change differs from the fixed, for any given time and scenario.

Changes in topography in Antarctica tend to reduce the accumulation and increase the ablation wherever it occurs, but the effect is quite small (static compared with fixed); however, changes in ice flow substantially increase the discharge in response to mass accumulation (dynamic compared with static in figure 7*a*). The ratio of the dynamic to the fixed (i.e. surface mass balance) calculation decreases with increasing mass gain. For a given change in mass due to increased accumulation, the offsetting dynamic effect is greatest in the scenario of smallest climate change, because the time-period concerned is longest, so the time-integral of the ice-flux change is largest. During the twenty-first century, our estimates of surface mass-balance change give up to 0.1 m of sea-level fall, which the dynamic effect would reduce by about 10%.

On Greenland, there are two effects. First, increased marginal ablation associated with a rise in temperature will lower the surface; because of the temperature lapse rate, this will feedback positively on the ablation increase. Second, the margins of the ice sheet will tend to retreat as the ice is exhausted, preferentially reducing the areas where ablation is greatest. The first effect is dominant, so the mass loss is increased when the geometry of the ice sheet is allowed to evolve (static compared with fixed in figure 7*b*). When ice flow is allowed to evolve as well, the surface altitude change will tend to steepen the slopes in the ablation zone, and thus increase the flux of ice from the accumulation to the ablation zone, while thinning of outlet glaciers will tend to reduce the rate of ice discharge (Huybrechts & De Wolde 1999). Both of these

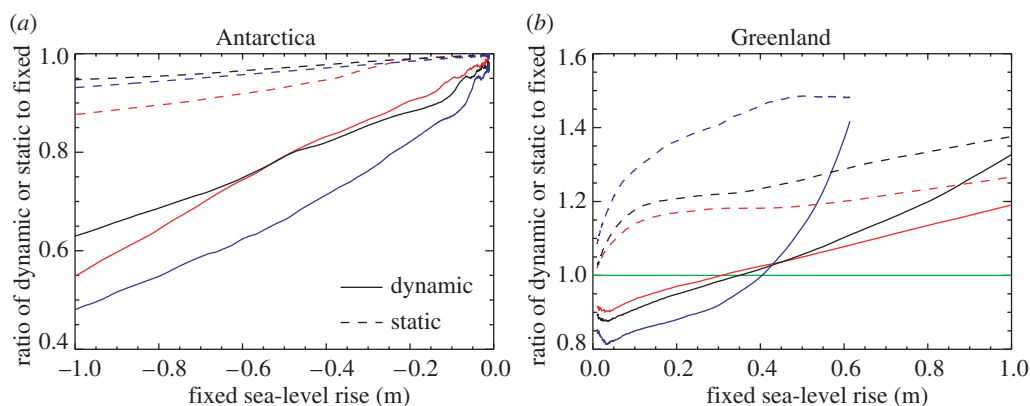


Figure 7. Effect of changes in ice-sheet dynamics and topography. Sea-level contribution from the ice sheets calculated, including changes in ice flow and topography ('dynamic') or only in topography ('static') plotted against the calculation for the change in surface mass balance alone ('fixed') from the results of Huybrechts & De Wolde (1999). The blue, black and red lines are for different CO<sub>2</sub> levels, in increasing order, so the blue has the least climate change and the red the most. The horizontal green line marks unity.

effects will give convergence in the ablation zone, offsetting some of the lowering of the surface and the consequent ablation increase (the first effect of topography change). These are negative dynamical feedbacks on loss of ice (dynamic compared with static). They alter the balance such that the loss of ablation area is the dominant effect initially, and there is less mass loss with evolving topography and flow than when both are constant (dynamic compared with fixed). The topographic and dynamical effects balance rather closely for mass loss of up to 0.5 m, so the dynamic and fixed calculations give results which differ by only 20% at most.

In these simulations, for the next few centuries, dynamical and topographic changes make the sea-level contribution from Greenland less positive and from Antarctica less negative. As discussed in §1 and reviewed by Alley *et al.* (2005), the possibility also exists of relatively rapid acceleration of ice flow in response to basal melting of ice shelves or perhaps runoff from ice sheets. Such effects are not included in current continental ice-sheet models like that of Huybrechts & De Wolde (1999), and would tend to make the contribution from both ice sheets more positive. Using a formulation of accelerated flow in Greenland resulting from surface runoff percolating to and lubricating the bed, Parizek & Alley (2004) suggested that it could add 0.15–0.40 m to the Greenland contribution by 2500, compared with the contribution of 0.4–3.2 m of Huybrechts & De Wolde (1999). Shepherd *et al.* (2004) estimated that accelerated discharge of West Antarctic ice streams contributed  $0.13 \pm 0.02$  mm yr<sup>-1</sup> to sea level during the 1990s. The middle of the range of our scenarios for surface mass-balance change for Antarctica is about  $-1.0$  mm yr<sup>-1</sup> at 2100 (figure 4a). In order for changes in Antarctica to have a net positive sum, therefore, this extra discharge would have to increase by a factor of between 5 and 10.

Because the ice sheets adjust over multi-millennial time-scales to previous climate change, it is possible that the ice-sheet mass balance was not zero in the initial climate (late nineteenth century), i.e. net surface mass balance did not

equal ice discharge then. Such slow adjustment would persist into the future as an additional term, but it is relatively small, at no more than a few  $0.1 \text{ mm yr}^{-1}$  (Church *et al.* 2001; Huybrechts *et al.* 2004).

## 9. Conclusions

Extending earlier work by Church *et al.* (2001) and Huybrechts *et al.* (2004), we have demonstrated a method for calculating changes in ice-sheet surface mass balance caused by future climate change and the resulting sea-level contribution. The method combines (i) annual time-series of change in temperature and precipitation averaged over each ice sheet simulated for future centuries by AOGCMs, which have relatively low spatial resolution, (ii) spatial and seasonal patterns of change simulated by high-resolution GCMs, (iii) observed climatologies, used instead of model control climatologies in order to minimize the effect of model bias and (iv) a surface mass-balance model at 20 km resolution calibrated against observations. The method is convenient because for each high-resolution model it involves calculating a single mass-balance perturbation table, which can then be used with any AOGCM scenario. Since AOGCMs consistently exhibit linear relationships between global-average temperature change and the magnitude of regional climate change, the method can easily be adapted to use with time-series of global-average temperature change, for instance produced by a simpler climate model.

We find that the uncertainty in the mass-balance perturbation is about 20% for Antarctica and 25% for Greenland, mostly associated with the pattern of climate change, on the basis of the four high-resolution models we have available. AOGCMs indicate that precipitation will increase with temperature for both ice sheets at *ca*  $5\% \text{ K}^{-1}$ , with some model spread. Since there is little surface ablation in Antarctica even in extreme scenarios, Antarctica contributes negatively to sea level on account of increased accumulation. Ablation rises nonlinearly with temperature on Greenland and more rapidly than accumulation, so Greenland contributes positively to sea level. The net contribution from the ice sheets due to surface mass-balance changes can be of either sign, depending on model and scenario.

Owing to the relatively small warming simulated in the margins of the Greenland ice sheet by the high-resolution models, the threshold in Greenland annual and area-average temperature change which produces a net negative surface mass balance is higher than previously estimated from simulations which assumed a uniform warming. The threshold is found to be  $4.5 \pm 0.9 \text{ K}$  in Greenland temperature change, and  $3.1 \pm 0.8 \text{ K}$  in global-average temperature change. For sustained warmings above this threshold, it is likely that the ice sheet would eventually be eliminated.

Changes in ice dynamics and surface topography were not considered and would modify these results. Those which can be simulated by existing continental ice-sheet models would tend to reduce the magnitude of the sea-level contribution in the next few centuries, by *ca* 20% in the twenty-first century. However, recent observations suggest that climate change could perhaps produce accelerated discharge of ice into the ocean, tending to increase the sea-

level contribution from both ice sheets. If the loss of ice were large from Antarctica, it might outweigh the increased accumulation there. Such effects have yet to be thoroughly understood and modelled.

We are grateful to Martin Wild for useful discussions, to Shawn Marshall and Ralf Greve for their helpful reviews and to Tony Payne and the Royal Society for organizing the meeting. Work at the Hadley Centre was supported by the UK Department for Environment, Food and Rural Affairs under contract PECD 7/12/37 and by the Government Meteorological Research and Development Programme. P.H. acknowledges support through the German HGF-Strategiefonds Projekt 2000/13 SEAL (Sea Level Change) and the Belgian Science Policy Office Second Programme on Global Change and Sustainable Development under contract EV/10/9B. The ECHAM5 T106 experiment was performed at ETH Zurich and supported by the Swiss National Supercomputing Centre CSCS. We acknowledge the international modelling groups for providing their data for analysis, the Program for Climate Model Diagnosis and Intercomparison (PCMDI) for collecting and archiving the model data, the JSC/CLIVAR Working Group on Coupled Modelling (WGCM) and their Coupled Model Intercomparison Project (CMIP) and Climate Simulation Panel for organizing the model data analysis activity, and the IPCC WG1 TSU for technical support. The IPCC Data Archive at Lawrence Livermore National Laboratory is supported by the Office of Science, US Department of Energy.

## References

- Allen, M. R. & Ingram, W. J. 2002 Constraints on future changes in climate and the hydrologic cycle. *Nature* **419**, 224–232. (doi:10.1038/nature01092)
- Alley, R. B., Clark, P. U., Huybrechts, P. & Joughin, I. 2005 Ice-sheet and sea-level changes. *Science* **310**, 456–460. (doi:10.1126/science.1114613)
- Box, J. E., Bromwich, D. H., Veenhuis, B. A., Bai, L.-S., Stroeve, J. C., Rogers, J. C., Steffen, K., Haran, T. & Wang, S.-H. In press. Greenland ice sheet surface mass balance variability (1988–2004) from calibrated Polar MM5 output. *J. Clim.*
- Church, J. A. & White, N. J. 2006 A 20th century acceleration in global sea level rise. *Geophys. Res. Lett.* **33**, L01602. (doi:10.1029/2005GL024826)
- Church, J. A., Gregory, J. M., Huybrechts, P., Kuhn, M., Lambeck, K., Nhuan, M.T., Qin, D. & Woodworth, P. L. 2001 Changes in sea level. In *Climate change 2001: the scientific basis. Contribution of Working Group I to the Third Assessment Report of the Intergovernmental Panel on Climate Change* (ed. J. T. Houghton, Y. Ding, D. J. Griggs, M. Noguer, P. van der Linden, X. Dai, K. Maskell & C. I. Johnson), pp. 639–693. Cambridge, UK: Cambridge University Press.
- Chylek, P. & Lohmann, U. 2005 Ratio of the Greenland to global temperature change: comparison of observations and climate modeling results. *Geophys. Res. Lett.* **32**, L14705. (doi:10.1029/2005GL023552)
- Cubasch, U., Meehl, G. A., Boer, G. J., Stouffer, R. J., Dix, M., Noda, A., Senior, C. A., Raper, S. C. B. & Yap, K. S. 2001 Projections of future climate change. In *Climate change 2001: the scientific basis. Contribution of Working Group I to the Third Assessment Report of the Intergovernmental Panel on Climate Change* (ed. J. T. Houghton, Y. Ding, D. J. Griggs, M. Noguer, P. van der Linden, X. Dai, K. Maskell & C. I. Johnson), pp. 525–582. Cambridge, UK: Cambridge University Press.
- Glover, R. W. 1999 Influence of spatial resolution and treatment of orography on GCM estimates of the surface mass balance of the Greenland ice sheet. *J. Clim.* **12**, 5510–5563. (doi:10.1175/1520-0442(1999)012<0551:IOSRAT>2.0.CO;2)
- Gregory, J. M. & Lowe, J. A. 2000 Predictions of global and regional sea-level rise using AOGCMs with and without flux adjustment. *Geophys. Res. Lett.* **27**, 3069–3072. (doi:10.1029/1999GL011228)

- Gregory, J. M., Huybrechts, P. & Raper, S. C. B. 2004 Threatened loss of the Greenland ice-sheet. *Nature* **428**, 616. (doi:10.1038/428616a)
- Gregory, J. M., Lowe, J. A. & Tett, S. F. B. In press. Simulated global-mean sea-level changes over the last half-millennium. *J. Clim.*
- Greve, R. 2000 On the response of the Greenland ice sheet to greenhouse climate change. *Clim. Change* **46**, 283–289. (doi:10.1023/A:1005647226590)
- Hanna, E., Huybrechts, P., Janssens, I., Cappelen, J., Steffen, K. & Stephens, A. 2005 Runoff and mass balance of the Greenland ice sheet: 1958–2003. *J. Geophys. Res.* **110**, D13108. (doi:10.1029/2004JD005641)
- Hasumi, H. & Emori, S. (eds) 2004 K-1 coupled GCM (MIROC) description. K-1 Technical Report no. 1, Center for Climate System Research, University of Tokyo.
- Holgate, S. J. & Woodworth, P. L. 2004 Evidence for enhanced coastal sea level rise during the 1990s. *Geophys. Res. Lett.* **31**, L07305. (doi:10.1029/2004GL019626)
- Huntingford, C. & Cox, P. M. 2000 An analogue model to derive additional climate change scenarios from existing GCM simulations. *Clim. Dyn.* **16**, 575–586. (doi:10.1007/s003820000067)
- Huybrechts, P. & De Wolde, J. 1999 The dynamic response of the Greenland and Antarctic ice sheets to multiple-century climatic warming. *J. Clim.* **12**, 2169–2188. (doi:10.1175/1520-0442(1999)012<2169:TDROTG>2.0.CO;2)
- Huybrechts, P., Letreguilly, A. & Reeh, N. 1991 The Greenland ice sheet and greenhouse warming. *Paleogeogr. Paleoclimatol. Paleoecol.* **89**, 399–412. (doi:10.1016/0031-0182(91)90174-P)
- Huybrechts, P., Gregory, J., Janssens, I. & Wild, M. 2004 Modelling Antarctic and Greenland volume changes during the 20th and 21st centuries forced by GCM time slice integrations. *Global Planet. Change* **42**, 83–105. (doi:10.1016/j.gloplacha.2003.11.011)
- Janssens, I. & Huybrechts, P. 2000 The treatment of meltwater retention in mass-balance parameterizations of the Greenland ice sheet. *Ann. Glaciol.* **31**, 133–140.
- Johannessen, O. M., Khvorostovsky, K., Miles, M. W. & Bobylev, L. P. 2005 Recent ice-sheet growth in the interior of Greenland. *Science* **310**, 1013–1015. (doi:10.1126/science.1115356)
- Johns, T. C. *et al.* 2003 Anthropogenic climate change for 1860 to 2100 simulated with the HadCM3 model under updated emissions scenarios. *Clim. Dyn.* **20**, 583–612. (doi:10.1007/s00382-002-0296-y)
- Kapsner, W. R., Alley, R. B., Shuman, C. A., Anandakrishnan, S. & Grootes, P. M. 1995 Dominant influence of atmospheric circulation on snow accumulation in Greenland over the last 18,000 years. *Nature* **373**, 52–54. (doi:10.1038/373052a0)
- Krabill, W. *et al.* 2004 Greenland ice sheet: increased coastal thinning. *Geophys. Res. Lett.* **31**, L24402. (doi:10.1029/2004GL021533)
- Krinner, G., Magand, O., Simmonds, I., Genthon, C. & Dufresne, J.-L. Submitted. Simulated Antarctic precipitation and surface mass balance at the end of the 20th and 21st centuries. *Clim. Dyn.*
- Murphy, B. F., Marsiat, I. & Valdes, P. 2002 Atmospheric contributions to the surface mass balance of Greenland in the HadAM3 atmospheric model. *J. Geophys. Res.* **107**, 4556. (doi:10.1029/2001JD000389)
- Nakićenović, N. *et al.* 2000 *Special report on emissions scenarios*, 599 pp. Cambridge, UK: Intergovernmental Panel on Climate Change.
- Oerlemans, J. & Fortuin, J. P. F. 1992 Sensitivity of glaciers and small ice caps to greenhouse warming. *Science* **258**, 115–117.
- Ohmura, A., Wild, M. & Bengtsson, L. 1996 A possible change in the mass balance of Greenland and Antarctic ice sheets in the coming century. *J. Clim.* **9**, 2124–2135. (doi:10.1175/1520-0442(1996)009<2124:APCIMB>2.0.CO;2)
- Parizek, B. R. & Alley, R. B. 2004 Implications of increased Greenland surface melt under global-warming scenarios: ice-sheet simulations. *Quaternary Sci. Rev.* **23**, 1013–1027. (doi:10.1016/j.quascirev.2003.12.024)

- Ridley, J., Huybrechts, P., Gregory, J. M. & Lowe, J. A. 2005 Elimination of the Greenland ice sheet in a high CO<sub>2</sub> climate. *J. Clim.* **18**, 3409–3427. (doi:10.1175/JCLI3482.1)
- Rignot, E. & Thomas, R. H. 2002 Mass balance of polar ice sheets. *Science* **297**, 1502–1506. (doi:10.1126/science.1073888)
- Shepherd, A., Wingham, D. & Rignot, E. 2004 Warm ocean is eroding West Antarctic ice sheet. *Geophys. Res. Lett.* **31**, L23402. (doi:10.1029/2004GL021106)
- Stott, P. A., Tett, S. F. B., Jones, G. S., Allen, M. R., Mitchell, J. F. B. & Jenkins, G. J. 2000 External control of twentieth century temperature by natural and anthropogenic causes. *Science* **290**, 2133–2137. (doi:10.1126/science.290.5499.2133)
- Van de Wal, R. S. W., Wild, M. & de Wolde, J. 2001 Short term volume change of the Greenland ice sheet in response to doubled CO<sub>2</sub> conditions. *Tellus* **53B**, 94–102.
- Van Lipzig, N. M., van Meijgaard, E. & Oerlemans, J. 2002 Temperature sensitivity of the Antarctic surface mass balance in a regional atmospheric climate model. *J. Clim.* **15**, 2758–2774. (doi:10.1175/1520-0442(2002)015<2758:TSOTAS>2.0.CO;2)
- Velicogna, I. & Wahr, J. 2005 Greenland mass balance from GRACE. *Geophys. Res. Lett.* **32**, L18505. (doi:10.1029/2005GL023955)
- Wild, M., Calanca, P., Scherrer, S. & Ohmura, A. 2003 Effects of polar ice sheets on global sea level in high resolution greenhouse scenarios. *J. Geophys. Res.* **108**, 4165. (10.1029/2002JD002451)
- Wild, M., Roesch, A., Tschuck, P. & Roeckner, E. 2004 ECHAM5 T106 time slice scenarios using PRUDENCE SST and SRES A2, B2 forcings. *Geophys. Res. Abstr.* **6**, 03537.

## NOTICE OF CORRECTION

The  $\Delta B$  threshold 95% confidence interval and the  $\Delta T_g$  threshold 95% confidence interval are now presented in their correct form.

A detailed erratum will appear at the end of the volume.

17 October 2006